The 2019 International Conference on Power Electronics (ICPE 2019 ECCE Asia)

Modeling and Experimental Verification of Geometry Effect on Core Losses

M. Mogorovic and D. Dujic

POWER ELECTRONICS LABORATORY
ÉCOLE POLYTECHNIQUE FÉDÉRALE DE LAUSANNE

Modeling And Experimental Verification of Geometry Effects on Core Losses

Marko Mogorovic and Drazen Dujic

Power Electronics Laboratory - PEL

École Polytechnique Fédérale de Lausanne - EPFL

Station 11, CH-1015 Lausanne

marko.mogorovic@epfl.ch, drazen.dujic@epfl.ch

Abstract—**This paper addresses the technical challenges of ferromagnetic core loss estimation for medium frequency transformers. While core losses are usually characterized from the manufacturer side for a given ferromagnetic material on a toroidal sample with sinusoidal excitation, these results are not necessarily directly transferable to typical conditions encountered within power electronic converters. Moreover, the presence of core cuts and its rectangular geometry with sharp corners have a significant influence on magnetic field distribution and therefore the localized loss density. A detailed analysis and modeling of the mentioned effects is presented in this paper together with experimental characterization of various core samples of interest considering both sinusoidal and square voltage excitation within the relevant frequency range. Derived models allow to generalize the core loss estimation based on characterization of one core sample to any different core shape and size made of the same material and same technology.**
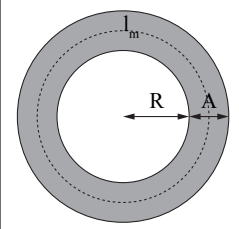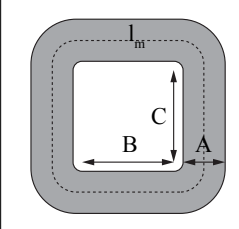
Nomenclature

l_m	Magnetic path Length
H_m	Peak magnetic field density
B_m	Peak flux density
K,α,β	Core Steinmetz coefficients
B_{sat}	Saturation flux density
μ_r	Relative magnetic permeability
μ_0	Magnetic permeability of vacuum
p_σ	Core loss density

I. Introduction

Regardless of the power or voltage range, magnetic components are a necessary part of any power electronic converter, having a significant impact on its efficiency and power density. Two main types of losses occur in magnetic components, core and winding losses. While for some components, such as DC filter inductors, core losses can be neglected, for others, such as transformers and AC inductors, they represent a significant portion of total losses and need to be properly addressed [1].

It is a common design approach to assume homogeneous magnetic induction field distribution within the transformer core volume. This allows for very simple core loss estimation and characterization. Core loss density distribution, as a direct function of the magnetic induction field, becomes uniform regardless of the core shape and size, thus neglecting the geometry effects on the total core loss. In other words, it is assumed that a toroidal and a rectangular core, as displayed in Table I, with same cross section ($A_t = A_r$) and magnetic path

TABLE I: Two most common core geometries

$l_m = 2(R + \frac{1}{2}A)\pi$	$l_m = 2(\frac{\pi}{2}A + B + C)$

length ($l_{mt} = l_{mr}$), with same excitation, would have the same total losses. This allows to directly transfer the conclusions, based on measurements on a small toroidal core sample, to any core shape and size with the given material.

Nevertheless, depending on the core shape and structure, this assumption does not hold in general. There have been some efforts to analyze the effect of geometry on various core properties: measurements in [2] experimentally quantify the influence of the core geometry on no-load loses on industrial distribution transformers in $[16-20]$ MVA power range. Work presented in [3] identifies and experimentally verifies the influence of various geometry ratios on total losses of toroidal cores; [4] offers analytic formulation and approximations of the partial differential equations used in FEM to estimate the fields and the loss distributions within the rectangular and toroidal cores with or without cuts; In [5], FEM is utilized to analyze the the effect of higher order excitation harmonics; Analysis of the possible accuracy improvement of electric simulations by including geometry based implications is described in [6].

This paper analyzes in detail the core structures of interest, as shown in Fig. 1, identifying and modeling the geometry related effects on magnetic field distribution and resulting core losses. Compared to the mentioned state of the art, radially laminated cores, typical for increasingly popular nanocrystalline and metglas materials, are included in the study. Moreover, the models derived in this work offer a direct relation between the core loss measurements on any specific core geometry sample to any different core geometry, made of the same material and with same technology.
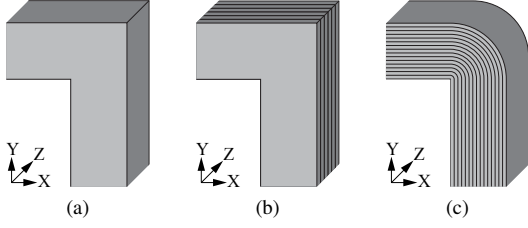
Fig. 1: Considered core structures: (a) isotropic; (b) axial lamination (in Z axis); (c) radial lamination;

II. FEM ANALYSIS

In order to identify the main effects of the core geometry, a detailed electromagnetic FEM analysis is performed on equivalent ($A_t = A_r, l_{mt} = l_{mr}$) parametrized rectangular and toroidal core models, as displayed in Fig. 2. Two intrinsically different core structures are considered: xy-isotropic (isotropic or axial laminated) and xy-anisotropic (radial laminated). It can be seen that the radial lamination has a significant influence on the magnetic induction field distribution. In contrast to xy-isotropic cores where magnetic reluctance is equal in all directions of the xy-plane, insulation (adhesive) gaps between the radially stacked ferromagnetic sheets represent a high re-

luctance path ("barrier") for the magnetic flux. Consequently, the average flux density is conserved along each ferromagnetic sheet path.

Plots of the magnetic induction field magnitude along a couple of radial lines, representative of the varying conditions within the given core sections are presented in Fig. 3. It can be seen that the field density distributions within the corner and straight regions of an xy-isotropic core are very different, whereas the average flux density within each sheet of a radially laminated core remains the same regardless of the region. Note that the variations from this average values in the corner regions are significantly smaller (negligible) in reality, as the lamination is roughly two orders of magnitude thinner compared to the ten-sheet downscaled model used in this study.

Comparing the average field densities within the lamination layers and the toroidal core, it can be concluded that a radially laminated rectangular core behaves exactly the same as its equivalent toroid core. On the other hand, it can be approximated that a rectangular xy-isotropic core behaves like a toroid with inner radius tending to zero in the corer regions, whereas the field density is uniformly distributed within its straight portions.
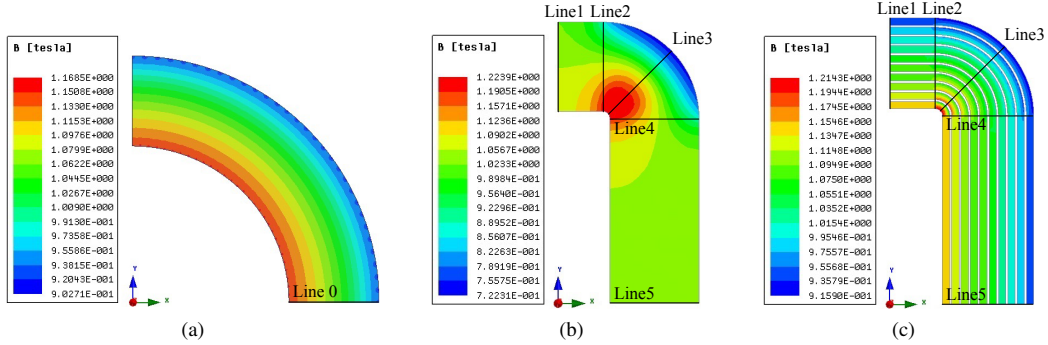

Fig. 2: Example of magnetic induction field distribution (B) within equivalent: (a) toroidal core, (b) rectangular xy-isotropic core (isotropic or laminated in Z axis) and (c) rectangular xy-anisotropic core (radial lamination; scaled down model to 10 sheets while maintaining the proportions), excited close to saturation (B_{sat})
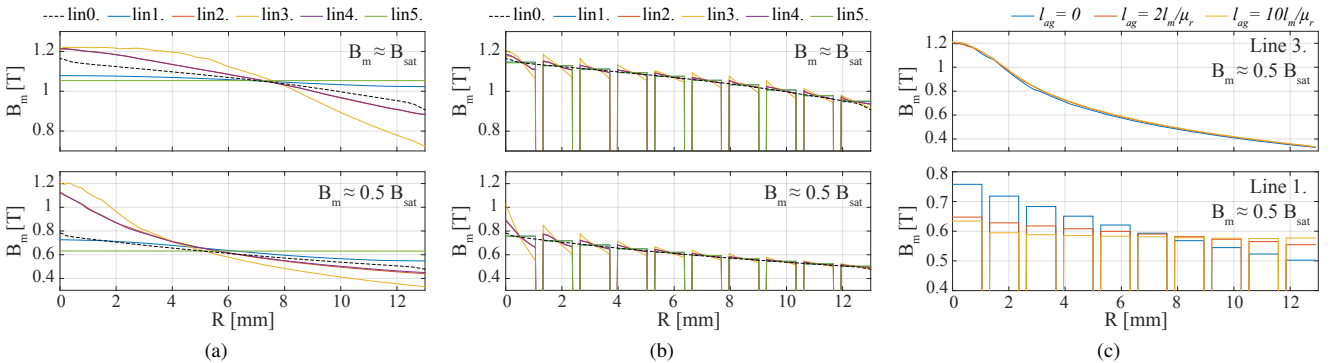

Fig. 3: Plots of the flux density magnitude along a couple of representative lines, as shown in Fig. 2, exposing the different field distribution in different core regions for: (a) toroid and xy-isotropic (isotropic or laminated in Z axis) rectangular core at 100% (top) and 50% (bottom) of the saturation induction (B_{sat}); (b) toroid and xy-anisotropic (radial laminated) rectangular core at 100% (top) and 50% (bottom) of B_{sat}; (c) rectangular xy-isotropic (top) and xy-anisotropic (bottom) cores with the presence of air-gap (l_{ag}) at 50% of B_{sat};

Moreover, it can be seen that the flux density has an effect on the field distribution. Magnetic reluctance of the material changes with the field density due to the nonlinear BH characteristic (saturation), thus causing the flux density redistribution.

Finally, air-gap has practically no effect on the flux distribution within xy-isotropic cores, whereas it causes the average field densities within the radial lamination layers of the xy-anisotropic cores to equalize, as shown in Fig. 3c. Depending on the size of the air-gap, a relatively large reluctance is added in series to the magnetic reluctance of each lamination path, thus rendering the reluctance difference of each path proportionally smaller. Consequently, the larger the air-gap, the more equal the flux distribution.

III. PROPOSED MODELING APPROACH

Based on the previous analysis, the proposed geometry dependent modeling of the field distribution within both the xy-isotropic and xy-anisotropic cores boils down to proper modeling of toroidal cores with various $K_t = A/R_m$ proportions at different flux density levels.

A generalized toroid core geometry detail is shown in Fig. 4. Starting from the analytic expression for the magnetic field within the infinitesimally narrow layer along the equi-magnetic-field intensity line of the toroid core

$$H_m(r) = \frac{NI_m}{2\pi r} \quad (1)$$

and taking into account the non-linear BH curve of the magnetic material, it is possible to reproduce the magnetic induction field density distribution within the generalized toroid core

$$B_m(r) = B_m(H_m(r))H_m(r) \quad (2)$$

where $B_m(H_m)$ represents the exact characteristic BH curve of the given material. This curve can either be obtained by means of characterization and directly sampled using interpolation, as shown in Fig. 5, or alternatively some BH curve model can be employed, such as described in [6], [7].
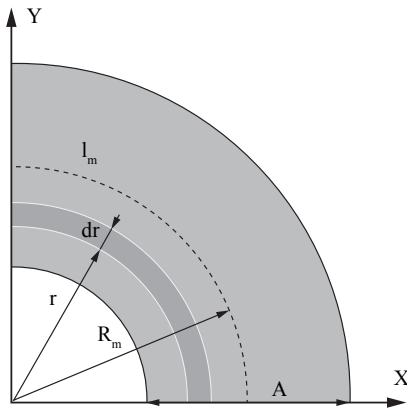
Moreover, it is assumed that the BH curve is frequency-independent within the normal operating frequency range for the given core. This assumption is typically true as the operation at frequencies high enough for μ_r to start to decrease is tied to a dramatic (usually unacceptable) increase of losses.

In order to enable the modeling using only the available manufacturer data-sheet data, an $\arctan$ based BH curve model is derived, similar to the procedure described in [7]. The form of the model is given in as

$$B_m(H_m) = C_1 \arctan(C_2 H_m) + \mu_0 H_m \quad (3)$$

where the constants C_1 and C_2 can be obtained from the two boundary conditions:

(i) Asymptotic convergence at high H_m

$$B_m(H_m \to \infty) = B_{sat} + \mu_0 H_m \quad (4)$$

Taking into account $\lim_{x \to \infty} \arctan(x) = \pi/2$, the first coefficient can be expressed as

$$C_1 = \frac{2B_{sat}}{\pi} \quad (5)$$

(ii) According to the definition of $\mu_r = B_{sat}/(\mu_0 H_{sat})$, H_{sat} is defined as a value of magnetic field where saturation level reaches 90%

$$B_m(H_{sat}) = 0.9B_{sat} \quad (6)$$

Substitution of (3) and (5) in (6) leads to

$$C_2 = \frac{\mu_0 \mu_r}{B_{sat}} \tan\left(\frac{0.9\pi}{2}\right) \quad (7)$$

As can be seen in Fig. 5, (3),(5) and (7) offer a sufficiently accurate BH curve model that utilizes only the available data-sheet information, i.e. μ_r and B_{sat}, that is used in the rest of the analysis in this paper.

According to original Steinmetz equation, the average core loss density within the entire core volume can be expressed as a function of frequency and flux density magnitude

$$p_{\sigma.avg} = Kf^\alpha B_{m.avg}^\beta. \quad (8)$$

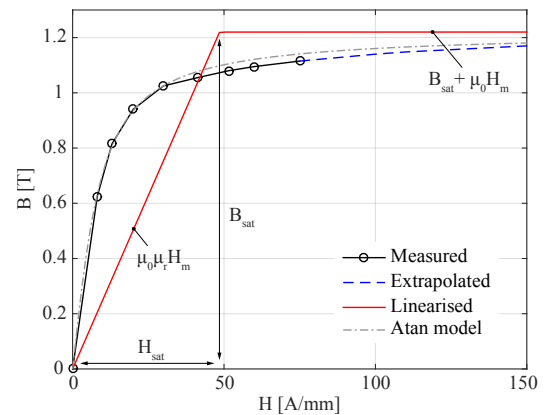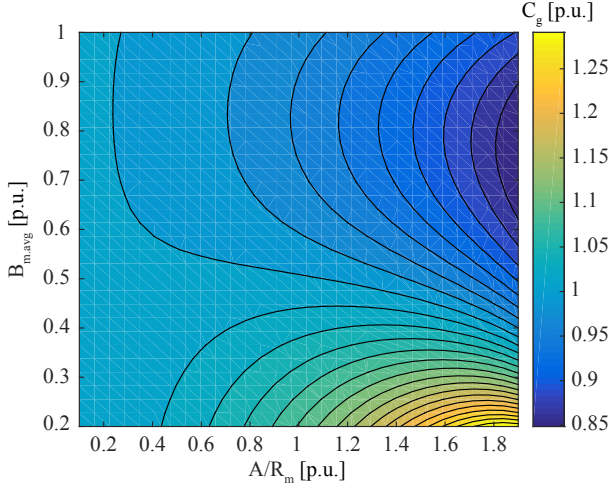Fig. 4: Geometry detail of a generalized toroid core

Fig. 5: BH curve of nanocrystalline - Finemet

Fig. 6: Map of the core loss geometry coefficient for the measured BH curve, as displayed in Fig. 5 and $\beta = 2.1$

Fig. 7: Multi-variable polynomial fitting of the geometry coefficient from Fig. 6 within the most important range, B_m from 0.4 to 1 T and A/R_m from 0.1 to 1.9 p.u. (a) Plots of the numeric calculation and polynomial fit of a representative family of curves within the described range. (b) Error histogram of the polynomial fit estimation referred to the numeric solution for a set of 100'000 points within the described range.

This leads to the geometry independent total per-length core losses

$$P'_{\sigma.tot} = p_{\sigma.avg} 2\pi R_m A. \qquad (9)$$

Note that a different core loss density model can be used as well - e.g. improved generalized Steinmetz equation (IGSE) [8] for non-sinusoidal excitation waveforms. For the sake of simplicity, the derivation in this paper is done with the original Steinmetz equation.

However, application of the Steinmetz, or some other selected equation on the flux density distribution function from (2) generates the geometry dependent core loss distribution

$$p_\sigma(r) = K f^\alpha B_m^\beta(r). \qquad (10)$$

A surface integral of this function leads to the total geometry-dependent per-length core losses

$$P'_{\sigma.tot.g} = \int_S p_\sigma ds = \int_{R_m-A/2}^{R_m+A/2} p_\sigma(r)\, 2\pi r\, dr. \qquad (11)$$

The geometry related effects on the core losses can be expressed with a geometry factor

$$C_g = \frac{P'_{\sigma.tot.g}}{P'_{\sigma.tot}}. \qquad (12)$$

Finally, substitution of (8), (9), (10) and (11) in (13) leads to

$$C_g = \frac{1}{R_m A B_{m.avg}^\beta} \int_{R_m-A/2}^{R_m+A/2} B_m^\beta(r) r\, dr. \qquad (13)$$

This integral requires numeric integration as $B_m^\beta(r)$ is a non-linear function whose integral cannot be analytically expressed. Numeric integration of (13) is performed with respect to (1) and (2) for all variations of $B_{m.avg}$ and A/R_m in their corresponding ranges of interest, from 0.2 to 1 T and from 0.1 to 1.9 p.u., respectively, thus generating a map of the geometric core loss coefficient, as displayed in Fig. 6.
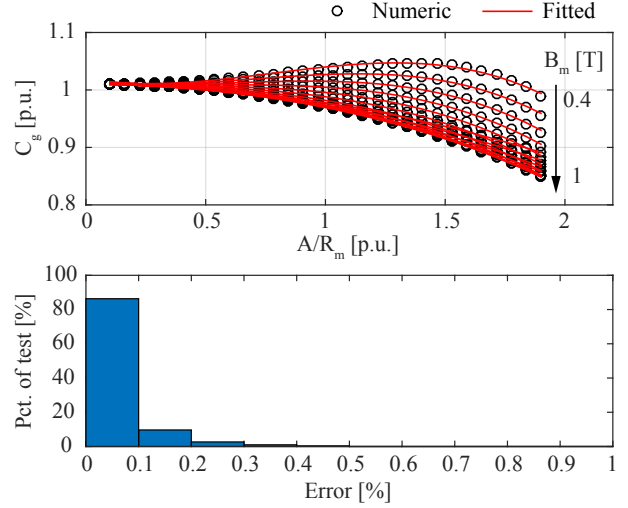
It can be seen that the total losses may vary roughly within the range of -20% to $+10\%$ compared to the averaged estimation, as given in (9). Moreover it is interesting to notice that the core losses increase with the increase of A/R_m at the light saturation ($B_{m.avg}$ in range 0.2 to 0.4 T) whereas the opposite is true at high saturation($B_{m.avg}$ in range 0.6 to 0.1 T). This is an expected result as the relative value of μ_r is very high at low $B_{m.avg}$, thus causing a significant increase of the local B_m as a result of the increased H_m in the inner regions of the core ($r < R_m$). This increase in B_m directly affects the local core loss density according to (10).

On the other hand, at high $B_{m.avg}$, μ_r is substantially lower, thus the local B_m increase within the inner regions of the core compared to $B_{m.avg}$ is not so pronounced. This effect can clearly be observed in Fig. 3a. Moreover, the local B_m in the outer core regions ($r > R_m$) decreases as a result of the decrease of H_m with higher μ_r, characteristic for decreased H_m. Qualitatively, this effect causes the local losses in the outer core region to decrease more than the ones in the inner core region increase compared to the averaged ones, thus resulting in a decrease of the total core losses. Therefore, the A/R_m influence on the losses is the most pronounced within the $B_{m.avg}$ region where relative change of the μ_r is the highest, between 0.8 and 0.9 T, as can be seen in Fig. 5.

In order to achieve good utilization of the ferromagnetic material and the magnetizing characteristic as linear as possible, the preferred B_m operation is usually slightly below the knee of the BH curve, between 0.5 and 0.9 T for the the given material, as displayed in Fig. 5. In order to facilitate a very fast model execution, required in design optimization applications [9], a third-order multi-variable polynomial fitting

(a)

Equivalent Circuit
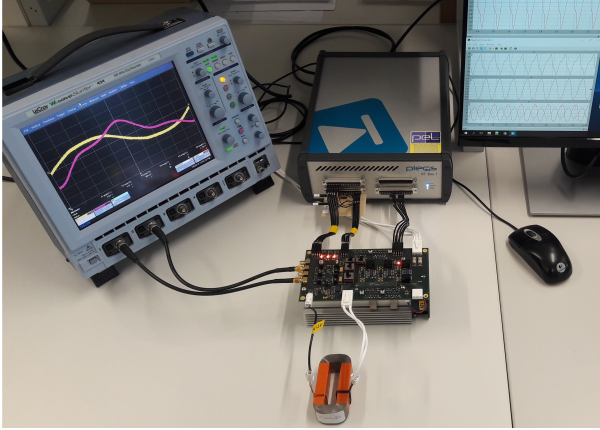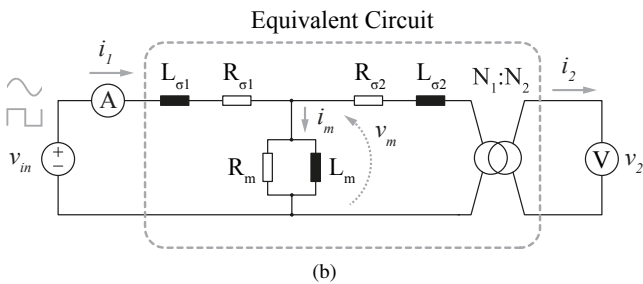
(b)

Fig. 8: Custom made core loss characterization setup capable of generating both sinusoidal and square voltage excitation in the frequency range of interest [11]: (a) Setup (b) Measurement scheme

Fig. 9: Custom made core samples for experimental verification. First two columns: toroidal core samples that cover a wide A/R_m geometry range. Last column: cut and uncut U cores with identical size and their equivalent toroidal core

of the geometric core loss coefficient, such as described in detail in [10], is performed on the results of the numeric calculation of 100'000 test points within the $B_{m.avg}$ range between 0.4 to $1\,\mathrm{T}$, as displayed in Fig. 7. It can be seen that a very accurate fit can be achieved within 0.5% error compared to the numeric solution.

The derived multi-variable polynomial model has the next form

$$C_g = \begin{bmatrix} B_m^3 \\ B_m^2 \\ B_m \\ 1 \end{bmatrix}^T \begin{bmatrix} A_m \end{bmatrix} \begin{bmatrix} (A/R_m)^3 \\ (A/R_m)^2 \\ (A/R_m) \\ 1 \end{bmatrix} \qquad (14)$$

where

$$A_m = \begin{bmatrix} 0.043 & -0.476 & 0.481 & -0.077 \\ -0.309 & 1.852 & -1.305 & 0.204 \\ 0.476 & -2.160 & 1.195 & -0.183 \\ -0.210 & 0.755 & -0.370 & 1.065 \end{bmatrix}. \qquad (15)$$

As can be seen, the evaluation of the derived multi-variable polynomial model boils down to a simple low-order matrix multiplication that executes extremely fast, two orders of magnitude compared to numeric integration.

Models for the xy-anisotropic rectangular cores are derived by simple application of the developed model on the equivalent toroidal core. On the other hand, modeling of rectangular xy-isotropic cores requires a breakdown into four straight segments with uniform flux density B_{avg}, and an equivalent torroid modeling the four corner elements.

IV. EXPERIMENTAL VERIFICATION

Experimental verification is performed to support the conclusions of the analysis and to verify the derived models. Core losses are measured using a custom made core loss characterization setup [11], as displayed in Fig. 8, on various core samples, as shown in Fig. 9. The measurement principle is depicted in Fig. 8b. Each of the core samples is equipped with two windings, comprising a transformer. Primary winding is excited with the controllable voltage source of the characterization setup, capable of generating both sinusoidal and custom square waveforms. Secondary side is in open circuit operation ($i_2 = 0\,\mathrm{A}$) - only the high-impedance voltage measurement interface is connected. Voltage measurement is therefore not sensitive to voltage drops on the winding resistance ($v_2 = v_m$). Current measurement on the other hand is performed via a shunt resistor on the primary side, thus ensuring the that there is no phase delay between the current ($i_1 = i_m$) and voltage (v_m) measurements, as given in Fig. 10.

A series of nanocrystalline toroidal and rectangular cut and uncut core samples, as given in Fig. 9, have been procured for the verification purposes of this study. This allows to make a proper breakdown of the influence of the core geometry. Identical toroidal cores featuring different A/R_m ratios, in range between 0.1 to 1.5 have been tested with sinusoidal excitation at $1\,\mathrm{kHz}$, as displayed in Fig. 11. All of the core loses are represented in p.u. relative to the core losses measured on the sample with extremely low $A/R_m = 0.1$ where the loss distribution can be considered constant, thus directly corresponding to the derived core loss geometry coefficient. It can be seen that the derived core geometry coefficient qualitatively captures the trend of the core losses, but still relatively large errors are present up to 28%. Nevertheless, it
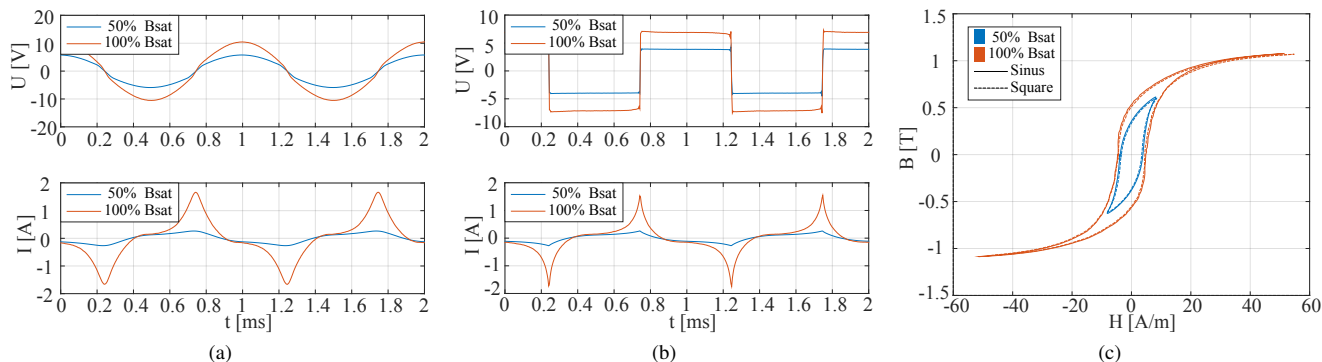
Fig. 10: Measured voltage (top) and current (bottom) plots for 50% and 100% of B_{sat} in case of sinusoidal (a) and square (b) wave excitation at 1 kHz, on a nanocrystalline core sample; (c) BH loops for all of the mentioned operating conditions;
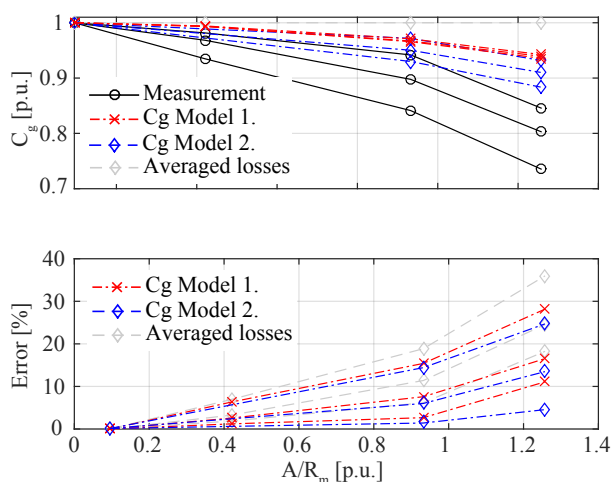

Fig. 11: Loss estimation and measurements on three toroidal core samples covering a wide A/R_m spectrum at three different saturation levels $B_m = 0.7, 0.8$ and 0.9 T at 1 kHz sinusoidal excitation. All of the core loses are represented in p.u. relative to the core losses measured on the sample with extremely low $A/R_m = 0.1$ where the loss distribution can be considered constant, thus directly corresponding to the derived core loss geometry coefficient. C_g model 1 and 2 refer to the core geometry coefficients obtained using the described arctan model and the exact BH measured curve characterized on the toroidal core sample with very low $A/R_m = 0.1$, respectively.

can still offer an accuracy improvement compared to the usual averaged loss model that completely neglects the geometry related effects. It can be seen that a slightly better result can be achieved using a real measured BH curve characterized on a toroidal core sample with a low A/R_m ratio. However, accuracy improvement is rather small, thus reinforcing the validity of the described arctan BH model.

The rectangular uncut core and its equivalent toroidal core have been tested in same conditions to verify the theoretical conclusions from the FEM analysis. However, in contrast to the expected, very similar/same losses, the losses within the uncut rectangular core were roughly double compared to the equivalent toroid. This may be due to the severe material strain during the manufacturing process (e.g. applied forces, possible

damage, etc.) which is known to have an effect on the resulting magnetic properties.

V. CONCLUSION

Core losses are one of the most important effects to be considered when designing any AC magnetic component - having direct impact on the efficiency and required cooling effort. While it is a common design approach to assume homogeneous magnetic induction field distribution within the transformer core volume, it has been shown that depending on the core shape and structure, this assumption does not hold in general.

Theoretical and FEM analysis of the magnetic and induction fields within the structure of the core have been performed. Major influencing factors have been identified and a mathematical description of the corresponding effect on the core losses has been provided. It has been shown how a computational cost of the resulting numerical model can be reduced (up to two orders of magnitude) to a simple low-order matrix multiplication via a multi-variable polynomial fitting within a slightly reduced variable range of interest.

Experimental verification was performed on the representative core samples. For the loss estimation on toroidal cores with various A/R_m ratios, an accuracy improvement of roughly 10% is achieved compared to the averaged loss density approach.

Nevertheless, the results of the loss measurements on the rectangular uncut core and its equivalent toroidal core did not match as theoretically expected. The increased losses within the rectangular core sample can most likely be attributed to the material stress during the manufacturing process which is known to have an effect on the resulting magnetic properties. Since this characterization was performed on only one core sample, this may not be a representative result. Additional measurements on more core samples are needed to characterize this effect with certainty and gain understanding of which are the most detrimental underlying factors. Furthermore, other core structures, i.e. isotropic and axial anisotropic, which do not experience this kind of material stress during manufacturing remain to be tested for these assumptions. This opens a topic for discussion and future work.

REFERENCES

[1] R. W. Erickson and D. Maksimovic, *Fundamentals of Power Electronics*, en. Springer US, Jan. 2001.

[2] J. Wojtkun, B. Bródka, and D. Stachowiak, "The influence of core geometry on no-load losses of medium power transformers," in *2018 International Interdisciplinary PhD Workshop (IIPhDW)*, May 2018, pp. 123–127.

[3] A. Kahveci, P. Szary, F. Herget, A. K. Putri, and K. Hameyer, "Methods for hysteresis losses determinations at non-standard ring core geometries equivalent to epstein measurements," in *2016 6th International Electric Drives Production Conference (EDPC)*, Nov. 2016, pp. 135–142.

[4] D. Robertson, "Magnetic Losses in Cores of Various Shapes," in *Nuclear Instruments and Methods 5 (1959) 133–141, North-Holland Publishing co.*.

[5] M. Puskarczyk, B. Jamieson, and W. Jurczak, "The influence of Core Shape and Material Nonlinearities to Corner Losses of Inductive Element," in *Excerpt from the Proceedings of the 2013 COMSOL Conference in Rotherdam*.

[6] M. Luo and D. Dujić, "Permeance based modelling of the core corners considering magnetic material nonlinearity," in *IECON 2015 - 41st Annual Conference of the IEEE Industrial Electronics Society*, Nov. 2015, pp. 000 950–000 955.

[7] C. Perez-Rojas, "Fitting saturation and hysteresis via arctangent functions," *IEEE Power Engineering Review*, vol. 20, no. 11, pp. 55–57, Nov. 2000.

[8] K. Venkatachalam, C. Sullivan, T. Abdallah, and H. Tacca, "Accurate prediction of ferrite core loss with nonsinusoidal waveforms using only Steinmetz parameters," in *Proc. of IEEE Workshop on Computers in Power Electronics*, Jun. 2002, pp. 36–41.

[9] M. Mogorovic and D. Dujic, "100kW, 10kHz Medium Frequency Transformer Design Optimization and Experimental Verification," in *IEEE Transactions on Power Electronics (early access)*.

[10] ——, "Computationally Efficient Leakage Inductance Estimation of Multi-Winding Medium Frequency Transformers," in *PCIM Europe 2019; International Exhibition and Conference for Power Electronics, Intelligent Motion, Renewable Energy and Energy Management*, May 2019.

[11] M. Luo, D. Dujic, and J. Allmeling, "Test Setup for Characterisation of Biased Magnetic Hysteresis Loopsin Power Electronic Applications," in *The 2018 International Power Electronics Conference (IPEC)*, Niigata, Japan, 2018., pp. 422–426.